ELSEVIER

Marine Chemistry 73 (2001) 273–290

MARINE CHEMISTRY

www.elsevier.nl/locate/marchem

An analysis of bomb radiocarbon trends in the Pacific

Amala Mahadevan [a,b,*]

[a] *Department of Earth Atmospheric and Planetary Sciences, MIT, Cambridge, MA 02139, USA*
[b] *Department of Earth and Planetary Sciences, Harvard University, Cambridge, MA 02139, USA*

Received 4 January 2000; received in revised form 3 November 2000; accepted 8 November 2000

Abstract

The post-nuclear time-series curves of $\Delta^{14}C$ from corals at different locations in the surface of the Pacific Ocean show a variation in the shape, amplitude and timing of the peak, with the subtropical records peaking first, followed by the western, and then eastern tropical records with lower maxima. This work takes an in-depth look at the processes that shape the time histories of $\Delta^{14}C$ in surface waters at different locations in the Pacific. A one-dimensional (1-D) model is used to examine whether convection and diffusion can delay the peaking of the $\Delta^{14}C$ time series. Using the three-dimensional (3-D) MIT general circulation model (GCM), the distribution and evolution of $\Delta^{14}C$ is simulated "offline" from 1955 onwards at 1° resolution globally. The GCM is used to tease apart the contribution of various processes, viz. advection, air–sea flux, convection and diffusion, to altering the $\Delta^{14}C$ content of surface waters at different locations in the Pacific. A time history of ^{14}C column inventories from the model is constructed to examine the role of horizontal advection in supplying tropical locations with ^{14}C much after the peak atmospheric flux. This model analysis supports the idea of ^{14}C-rich waters from the subtropics being transported to the western tropics via the subsurface, and then being advected eastward in the equatorial undercurrent and upwelled in the east.

Keywords: Radiocarbon; MIT-GCM; Pacific Ocean

1. Introduction

The radiocarbon isotope of carbon (^{14}C), which a half-life of 5730 years, occurs naturally in the atmosphere where it is continually formed by the neutron bombardment of ^{14}N atoms. ^{14}C enters the ocean through gas exchange with an equilibration time of 7–10 years, yielding an approximate steady state value in the atmosphere and ocean over long time periods. In the 1950s and 1960s however, the atmospheric testing of nuclear weapons added a large amount of ^{14}C into the atmosphere, approximately doubling the prebomb amount. The gradual infusion and spread of this ^{14}C through the oceans since the 1950s has provided a unique opportunity to study both the air–sea transfer of a tracer and the circulation of the oceans. Insight into its uptake and dissemination in the oceans can be particularly valuable in addressing questions about vertical mixing and lateral movement of water in the oceans. The concentration of ^{14}C is reported as $\Delta^{14}C$, the deviation of

* Atmospheric and Environmental Research 131 Hartwell Avenue, Lexington, MA 02421, USA. Tel.: +1-781-761-2288; fax: +1-781-761-2299.

0304-4203/01/$ - see front matter
PII: S0304-4203(00)00113-4

the $^{14}C/^{12}C$ ratio in a sample from its pre-industrial value, expressed in per mil (‰).[1]

Several modeling studies (Toggweiler et al., 1989a; Duffy et al., 1995; Follows and Marshall, 1996; Rodgers et al., 1997, 2000) have attempted to characterize the distribution and variation of $\Delta^{14}C$ in the oceans. The GEOSECS, INDIGO, WOCE and TTO observational programs provide good descriptions of the large-scale distribution of $\Delta^{14}C$ in the world's oceans at the time these surveys were conducted and are useful for model comparison. Changes to ^{14}C water column inventories in the interim between surveys have been used to estimate the large-scale horizontal transport in the ocean (Wunsch, 1984; Broecker et al., 1985; Peng et al., 1998). But besides the surveys, which provide snapshot views of the $\Delta^{14}C$ distribution, the time histories of the $\Delta^{14}C$ of surface water recorded in corals (Druffel, 1987; Toggweiler et al., 1991; Guilderson et al., 1998) exhibit interesting differences in how the $\Delta^{14}C$ value has grown, peaked and declined at different locations on the ocean's surface (Fig. 1a). While the atmospheric $\Delta^{14}C$ record rose sharply from 1955 onwards attaining a maximum value in the 1960s (inset, Fig. 1c), the ocean responded much more slowly on account of the long equilibration time of $^{14}CO_2$ in water. The subtropical gyres were the quickest to respond. The coral $\Delta^{14}C$ time series from French Frigate Shoals (Druffel, 1987) in the northern subtropical Pacific attained its maximum value in the early 1970s, with the record from Fiji (Toggweiler et al., 1991) in the southern subtropical Pacific reaching a lower maximum at about the same time. The coral records from tropical surface waters indicate a much more gradual increase in $\Delta^{14}C$. The western tropical Pacific record from Nauru (Guilderson et al., 1998) reaches a maximum in the mid 1980s, whereas the $\Delta^{14}C$ value recorded at Galapagos (Guilderson and Schrag, 1998) in the eastern tropics shows a steady rising trend that most likely continues well into the 1990s.

Winds in the subtropics are stronger than in the tropics, and there is a greater influx of ^{14}C from the atmosphere into the subtropics than at the equator. Further, upwelling dilutes the surface waters in the tropics with low $\Delta^{14}C$ subsurface water and consequently $\Delta^{14}C$ values are much lower in tropical surface waters. But, the tropical $\Delta^{14}C$ coral records continue to rise, peaking much later than the atmosphere or subtropical ocean, indicating a longer lasting or later acting source of ^{14}C in this region. It has been suggested that ^{14}C-rich water subducted in the subtropical gyres, gradually makes its way via the subsurface to the tropics, more specifically into the western tropics. From here, it is conveyed eastward in the equatorial undercurrent to furnish the water that is upwelling to the surface in the eastern tropics with additional ^{14}C. These ideas of upwelling, large-scale transport and exchange between the subtropics and tropics have been explored in several studies. Quay et al. (1983) conjectured from the analysis of the NORPAX (Leg 3) data that equatorial surface waters were low in $\Delta^{14}C$ because they were diluted by upwelling of low $\Delta^{14}C$ water from the subsurface. They concluded that the tropical $\Delta^{14}C$ values continued to rise long after other locations because of the equatorward meridional transport of ^{14}C from the subsurface tongues of high $\Delta^{14}C$ water to the north and south, seen in a meridional section. Druffel (1987) performed an analysis of the coral time histories at various Pacific sites using a simple model and concluded that meridional transport was responsible for the different time histories. For example, trans-equatorial Ekman transport was responsible for the offset in seasonal $\Delta^{14}C$ minima of different tropical coral time histories. Toggweiler et al. (1991) also performed such analyses using coral time histories and the output of an earlier simulation (Toggweiler et al., 1989a). Similar discussions of gyre and inter-gyre transport have been made in many contexts—Fine et al. (1987) in regard to tritium, Toggweiler and Carson (1995) for nitrate, Toggweiler et al. (1989b) for prebomb ^{14}C, Deser et al. (1996), Gu and Philander (1997), Zhang et al. (1998) in the

[1] The quantity

$$\delta^{14}C \equiv \left(\frac{\gamma}{\gamma_S} - 1\right) \times 1000, \tag{1.1}$$

where γ is the ratio of ^{14}C to ^{12}C concentration and γ_S is a standard pre-industrial ratio of ^{14}C to ^{12}C concentration, is further subject to a slight correction for isotope fractionation between ^{14}C and ^{13}C as follows (Stuiver and Polach, 1977)

$$\Delta^{14}C = \delta^{14}C - 2(\delta^{13}C + 25)\left(1 + \frac{\delta^{14}C}{1000}\right). \tag{1.2}$$

context of ocean temperatures and climatic variations, and more recently, Rodgers et al. (2000) and Guilderson et al. (1998) in regard to bomb-produced ^{14}C. Rodgers et al. (2000) performed a primitive equation model simulation of the Pacific with high resolution in the tropics and examined the effect of different Indonesian throughflows on the time histories of $\Delta^{14}C$ at different locations.

The present study was motivated by wanting to take an in-depth look into the processes contributing to the change in $\Delta^{14}C$ in surface waters at different locations in the Pacific. Is horizontal transport in the ocean the sole reason for the delayed peak in the time histories of coral $\Delta^{14}C$? A simple one-dimensional model is used to test whether processes such as convection and diffusion can also delay the peaking of $\Delta^{14}C$ time series in the surface ocean. Other processes are explored within a general circulation model (GCM). The flow fields from the MIT three-dimensional (3-D) global circulation model (MIT-GCM) and its machinery are used to model the post-nuclear oceanic radiocarbon distribution 'off-line' at a global resolution of 1°. The offline calculation enables us to (a) affordably model the radiocarbon globally at high resolution, and (b) eliminate processes in the model while maintaining the underlying velocity, temperature and salinity fields in the ocean. Thus, performing a three-dimensional simulation of $\Delta^{14}C$ in the global ocean with the MIT-GCM, we tease apart various processes (viz. horizontal and vertical advection, convection, diffusion and isopycnal mixing) in the model to identify the relative importance of each in changing the surface $\Delta^{14}C$ content at different locations. This enables us to identify, for example, the relative importance of upwelling in the eastern tropical Pacific as a means of diluting the surface ^{14}C. By constructing a time history of bomb ^{14}C column inventories at the different sites, we evaluate the extent to which inter-gyre transport or large-scale advection is responsible for a continued supply ^{14}C to the tropical sites long after atmospheric input has waned. While there have been several simulations of $\Delta^{14}C$ in the ocean, this particular study emphasizes examining the various processes affecting the concentration of a tracer subject to air–sea transfer in the surface ocean. An alternative approach to using a GCM for this kind of a study would be to perform flux balances using hydrographical data and box models for the different regions.

In what follows, I briefly describe the offline three-dimensional global circulation model for $\Delta^{14}C$ in Section 2. In Section 3, I present results from the GCM. Section 4 describes studies to diagnose the contribution of various processes to the pattern of $\Delta^{14}C$ evolution and distribution in the oceans. These include one-dimensional modeling, tracking the various terms in the evolution equation for $\Delta^{14}C$ during the GCM run, and a calculation of the bomb-^{14}C column inventory time series at certain locations. The findings are summarized in Section 5. Since $\Delta^{14}C$ is used as a tracer in the models, I sometimes use the terms ^{14}C and $\Delta^{14}C$ interchangeably in the context of the modeling.

2. General circulation model description

2.1. Dynamical model fields

Mean monthly values of velocities, temperature, salinity and convective index were saved from a run of the MIT-GCM (Marshall et al., 1997a,b) for the 9-year period 1987–1995. The model was run at $1 \times 1°$ resolution on a global domain extending from 80°S to 80°N. It was initialized with Levitus and Boyer (1994) hydrography and spun up for 8 years prior to the 1987–1995 period. The model uses a maximum of 21 layers in the vertical that range in thickness from 25 m at the surface to 500 m at depth. During the period 1987–1995, the model was driven with 12-hourly wind stresses and surface heat fluxes from the NCEP reanalysis data set (Kalnay et al., 1996) and simultaneously restored to Levitus and Boyer (1994) mean monthly temperature and salinity values in the surface. Gravitational stability was restored using simple convective overturning and the convective index (a value between 0 and 1 indicating the fraction of time any grid cell convected with the one below) was stored for each cell. Unresolved eddy processes were parameterized using the Griffies (1998) formulation of the Gent and McWilliams (1990) scheme in conjunction with Redi (1982) isoneutral mixing (henceforth referred to as the GM parameterization). Minimal constant eddy diffusivities of 10^3 m^2 s^{-1} in the horizontal and 10^{-5} m^2

s^{-1} in the vertical were used in addition. The model reproduced the global circulation reasonably well. A climatology was constructed from this model run by averaging the monthly mean model outputs over the

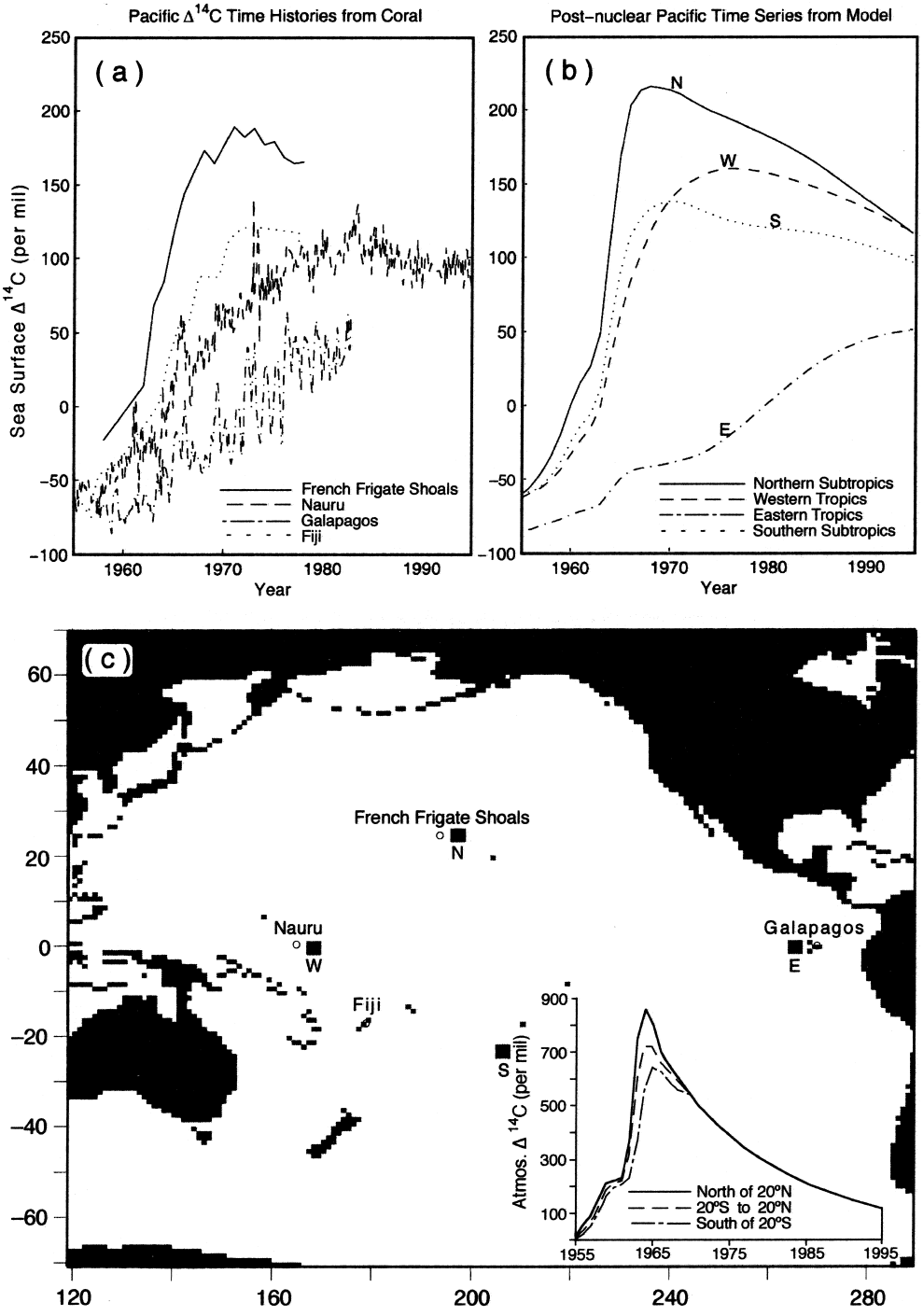

9-year period. These monthly climatological fields were used to model the radiocarbon distribution.

2.2. Modeling

The $\Delta^{14}C$ values in the ocean are initialized to a prebomb value using the Conkright et al. (1994) global silica distribution and the linear relationship between dissolved silica and $\Delta^{14}C$ postulated by Broecker et al. (1995) as

$$\Delta^{14}C = -70 - SiO_2, \quad (2.3)$$

where SiO_2 is in mmol/kg and $\Delta^{14}C$ is expressed in per mil. The relationship is found to hold fairly well in most regions other than in the Antarctic Circumpolar current (Broecker et al., 1995). The model is allowed to evolve from this initial distribution of $\Delta^{14}C$ into a prebomb state by running for a period of 20 years. This enables the surface $\Delta^{14}C$ values to equilibrate with the flow field. During this time the atmospheric value of $\Delta^{14}C$ is taken to be 0, the prebomb value. The Suess effect, i.e. the lowering of atmospheric $\Delta^{14}C$ to negative values prior to the 1950s through fossil fuel burning, is neglected during the spin up of the initial condition. Air–sea fluxes are computed as described in Section 2.3. The $\Delta^{14}C$ distribution at the end of this 20-year period is used as the initial condition for the post-nuclear model run that is begun in 1955 and integrated forward for 41 years.

$\Delta^{14}C$ is modeled as a passive tracer that is advected in the ocean. Its half-life is so much longer than the period modeled (41 years) that radioactive decay is neglected. The time evolution of the $\Delta^{14}C$ is governed by the equation

$$\frac{\partial \Delta^{14}C}{\partial t} = -u_H \cdot \nabla_H \Delta^{14}C - w\partial_z \Delta^{14}C + \nabla \cdot \left(K_{GM} \nabla \Delta^{14}C\right) + K_z \partial_{zz} \Delta^{14}C + \text{convection} + F_{a-s|surface} \quad (2.4)$$

where u_H is the horizontal velocity, w is the vertical velocity, K_{GM} is a mixing tensor, K_z is the vertical eddy viscosity coefficient, 'convection' represents convective mixing which is performed by mixing the contents of a cell with that below for a certain percentage (specified by its convective index) of the time steps, and F_{a-s} is the air–sea flux acting at the surface modeled as described below in Eq. (2.6). I use the same GM mixing scheme as used in the dynamical model along with a background vertical eddy diffusivity, K_z of 10^{-5} m^2 s^{-1} and no background horizontal diffusivity. The model domain extends from 80°S to 80°N with solid boundaries imposed at both 80°N and 80°S.

The model uses a finite volume formulation. Advection is computed in flux form, whereby the tracer fluxes at each cuboidal cell face are computed as the product of the cell-face area, the velocity (defined at the cell-face) and the tracer value at the face evaluated as the mean value of the adjoining two cells. The net advective effect is computed using central differencing via a flux balance for each grid cell.

The same Adams–Bashforth time stepping scheme is used for the tracer integration as in the dynamical model, with a time step of 8 h to ensure numerical stability. The monthly values of velocity, temperature, salinity, convective index, and the GM coeffi-

Fig. 1. Time histories of the $\Delta^{14}C$ in surface waters (a) recorded from coral and (b) from the surface layer of the GCM, at different sites in the Pacific shown marked in (c). The coral records at French Frigate Shoals, Nauru, Galapagos and Fiji are taken from Druffel (1987), Guilderson et al. (1998), Guilderson and Schrag (1998) and Toggweiler et al. (1991), respectively. The model values at each location (N, W, E, S) are averaged over a $3 \times 3°$ square consisting of nine grid cells. The subtropical sites peak earlier. The values at equatorial sites rise more slowly and peak later, the delay increasing from west to east in the tropics. Zonal atmospheric values of $\Delta^{14}C$ between 1955 and 1995 are shown inset in (c).

cients (calculated from the slope of the neutral surfaces) are held constant for the period of each month.

2.3. Air–sea exchange

The atmospheric distribution of radiocarbon is fairly uniform, except for some meridional variability that is accounted for by using slightly different time-series curves (inset, Fig. 1c) for the southern, equatorial and northern zones (Broecker et al., 1985). The air–sea transfer of $\Delta^{14}C$ is modeled using a gas exchange coefficient or piston velocity, k (in cm h^{-1}), calculated empirically (Wanninkhof, 1992) as

$$k = 0.39 u_{av}^2 (Sc/660)^{-1/2}, \quad (2.5)$$

where Sc, the Schmidt number, is computed using a third-order polynomial in temperature (cf. Appendix of Wanninkhof, 1992, e.g. $Sc = 524.54$ for CO_2 in seawater at a temperature of 25°C), and u_{av} is the average climatological wind speed at 10 m height in m s^{-1}. The air–sea flux or invasion rate of $\Delta^{14}C$, F_{a-s} (in per mil s^{-1}), is computed as

$$F_{a-s} = \alpha \frac{k}{\Delta z} \left(\Delta^{14}C_{at} - \Delta^{14}C_{surf} \right), \quad (2.6)$$

where $\Delta^{14}C_{at}$ and $\Delta^{14}C_{surf}$ are the value of $\Delta^{14}C$ in the atmosphere and surface ocean, respectively, Δz is the depth of the uppermost layer in the ocean model, k is converted to appropriate units (m s^{-1}), and α approximates the relative concentration of dissolved CO_2 to total dissolved inorganic carbon (DIC). I take α to have a uniform value of 0.005 (Follows and Marshall, 1996) as accounting for its variations would make little difference to the air–sea flux.

The use of monthly mean zonal and meridional components of the wind velocity to compute the wind speed results in rather low piston velocities as evidenced from the low surface $\Delta^{14}C$ values in the simulations, as well as a low global average compared with the bomb ^{14}C-based (Broecker et al., 1985) value of 21.2 ± 0.5 cm h^{-1} (Wanninkhof, 1992). Eq. (2.5) is extremely sensitive to the wind speed and in order to obtain sufficiently high piston velocities one has to compute the 6-hourly wind speed from the NCEP reanalysis winds and then average these over the month. This results in higher monthly mean wind speeds and consequently substantially higher piston velocities that seem more appropriate, and are hence used in the simulations described here. The piston velocity varies significantly in space and in time, resulting in a considerable variability in air–sea fluxes.

I choose four Pacific sites (marked N, W, E and S in Fig. 1c), one in the central north subtropical Pacific, one each in the western and eastern equatorial Pacific, and one in the central south subtropical Pacific, at which I compare the time histories of $\Delta^{14}C$ with coral records from nearby sites. These model sites are used for analyses and are chosen to be at least a few grid points away from land so that they may be free from any boundary effects in the numerical solution. In order that the $\Delta^{14}C$ values are not unduly biased by any peculiarities at a specific grid point in the model, the records for each of these sites are averaged over a $3 \times 3°$ square region consisting of nine grid cells in the plan view.

3. GCM results

The model simulation uses higher spatial resolution (1° globally) and better resolved heat and momentum fluxes in time than most earlier simulations. Since the horizontal mixing in the model is along isopycnal surfaces rather than horizontal planes, it does not produce the spurious upwelling inshore of the western boundary currents (Veronis, 1975) seen in some of the earlier models (Toggweiler et al., 1989a). It produces a fairly realistic subsurface advection as evidenced from the time series of bomb-^{14}C column inventories. The quality of the simulation is therefore quite good (Toggweiler, 2000, personal communication) in comparison to previous simulations. Various aspects of it are discussed in the following paragraphs.

3.1. $\Delta^{14}C$ distribution

In Fig. 2, the surface bomb $\Delta^{14}C$ distribution is plotted at the end of 1973, around the time of the GEOSECS survey and compared with the GEOSECS data. The model reproduces the large-scale $\Delta^{14}C$ distribution and the west-to-east gradient in the sur-

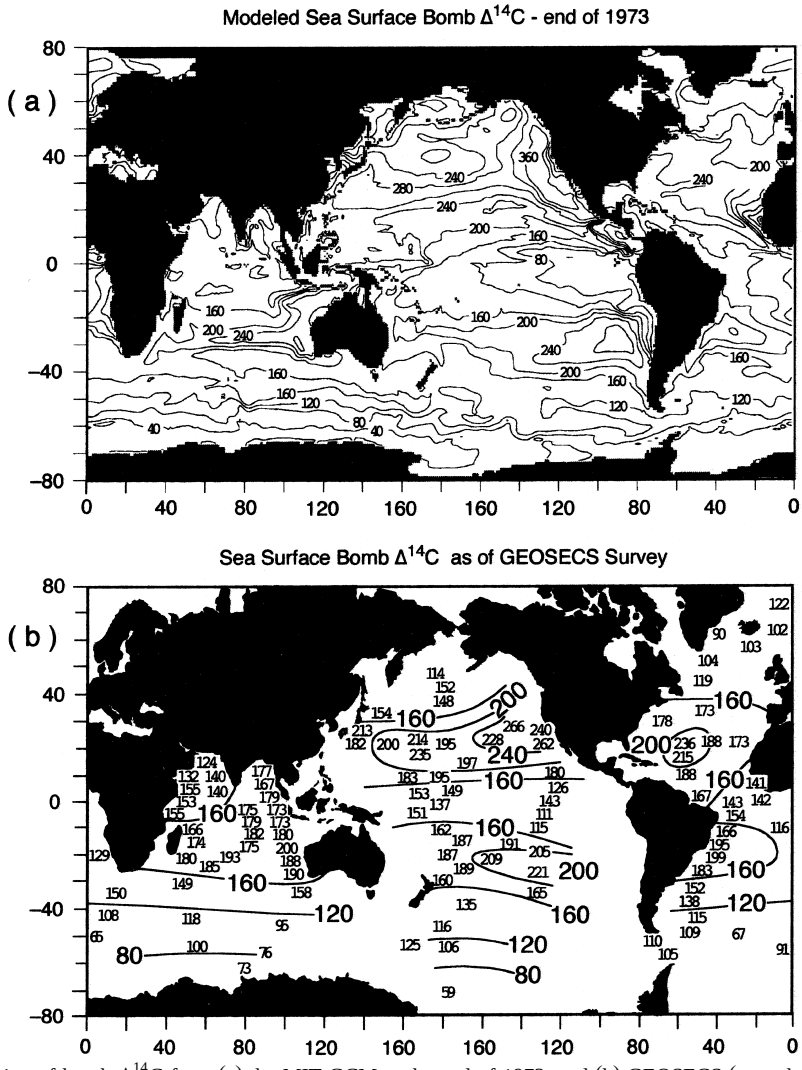

Fig. 2. Surface distribution of bomb $\Delta^{14}C$ from (a) the MIT-GCM at the end of 1973, and (b) GEOSECS (reproduced from Toggweiler et al., 1989a).

face Pacific. However, it develops unrealistically high pools of surface $\Delta^{14}C$ values in the eastern subtropical gyres. This seems to be a characteristic of other models too (Toggweiler et al., 1989a; Rodgers et al., 2000). The problem is striking in the eastern subtropical north Pacific. The density structure of the model shows tongue-shaped outcropping isopycnal surfaces in this region, indicating a shallow mixed layer. It is possible that the model has insufficient convective mixing in the northeastern subtropical Pacific, resulting in a shallow mixed layer and excessive pooling of ^{14}C in the surface.

A vertical section of $\Delta^{14}C$ from the model in Fig. 3, superimposed on the Western Pacific GEOSECS section shows that at most latitudes, the vertical penetration of ^{14}C calculated by the model reproduces the GEOSECS data fairly well. Between 30°S and 40°S, the data show approximately 100 m deeper penetration than predicted by the model. This is an improvement over what is seen in some other simu-

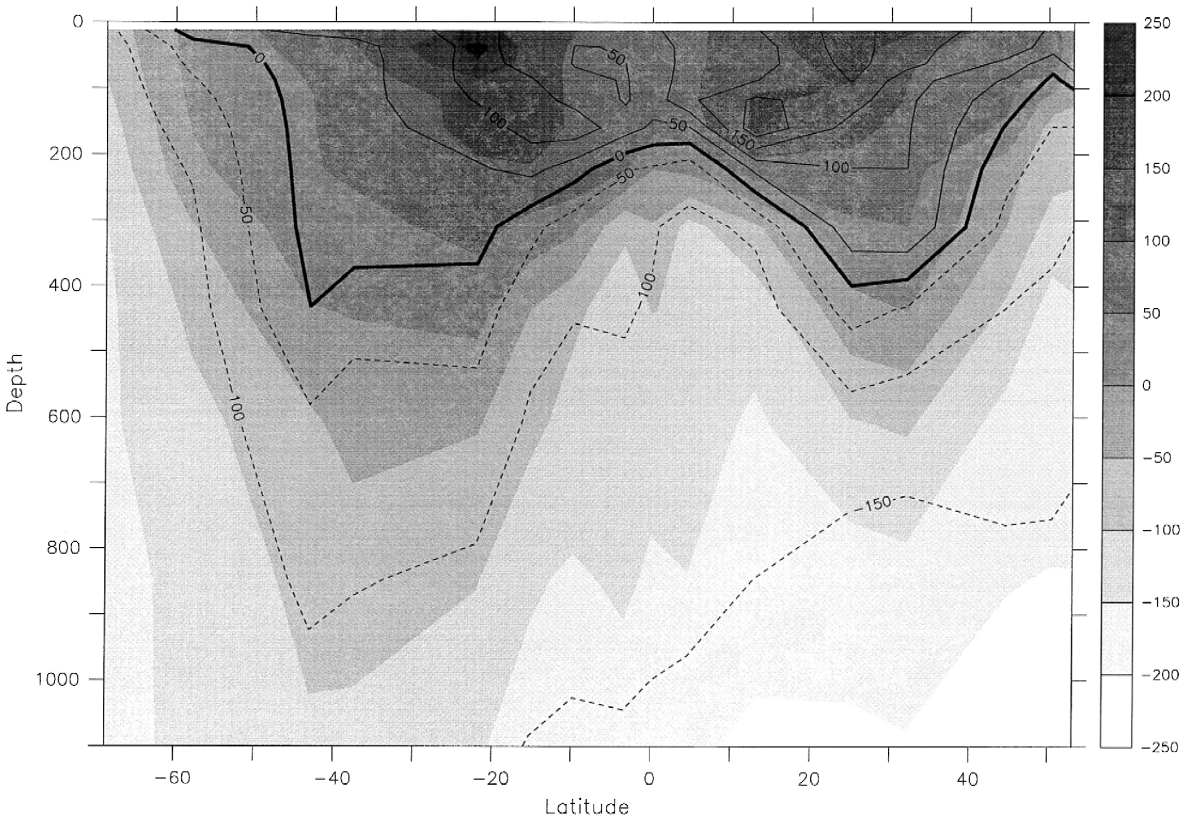

Fig. 3. Vertical section showing contours (solid and dotted lines) of $\Delta^{14}C$ in the top 1000 m of the MIT-GCM at the end of 1973. The section is formed by profiles taken at stations coinciding with those from the GEOSECS western Pacific tract at approximately 180°W. The GEOSECS values, recorded in 1974, are interpolated onto the model grid and fill-contoured in shades of grey. The values at boundaries between shaded grey regions are written on the plot for clarity.

lations (Rodgers et al., 2000) that tend to underpredict the penetration depth of the bomb ^{14}C signal.

3.2. Inventories

Bomb-produced ^{14}C column inventories in the model are computed using the expression

$$I = \frac{N_A \gamma_S \Sigma C \rho}{1000} \int_b^h \Delta_B{}^{14}C \, dz, \qquad (3.7)$$

where I is the column inventory in atoms/m^2, N_A is Avogadro's number, $\gamma_S = 1.18 \times 10^{-12}$ is the standard ratio of ^{14}C to ^{12}C (Stuiver et al. 1981), ΣC is the concentration of dissolved inorganic carbon in the ocean and is taken to be a constant value 2×10^{-3} mol/kg, ρ is the density of seawater also taken to be constant and equal to 1025 kg/m^3, $\Delta_B{}^{14}C$ is the difference between $\Delta^{14}C$ and prebomb-$\Delta^{14}C$ values, and the limits of integration refer to the ocean bottom and free surface. The above expression is derived neglecting the minor correction for isotopic fractionation in the definition of $\Delta^{14}C$, and treating it to be equivalent to $\delta^{14}C$ defined in (1.1).

Fig. 4 shows a snapshot of column inventories computed from the model at the end of 1973 alongside those from GEOSECS. In the subtropical gyres, there is a west-to-east gradient in the column inventory values of the model that is contrary to the east-to-west gradient observed in GEOSECS. This is consistent with the anomalously high surface $\Delta^{14}C$ values produced by the model in the western subtropical Pacific. Follows and Marshall (1996) ascribe

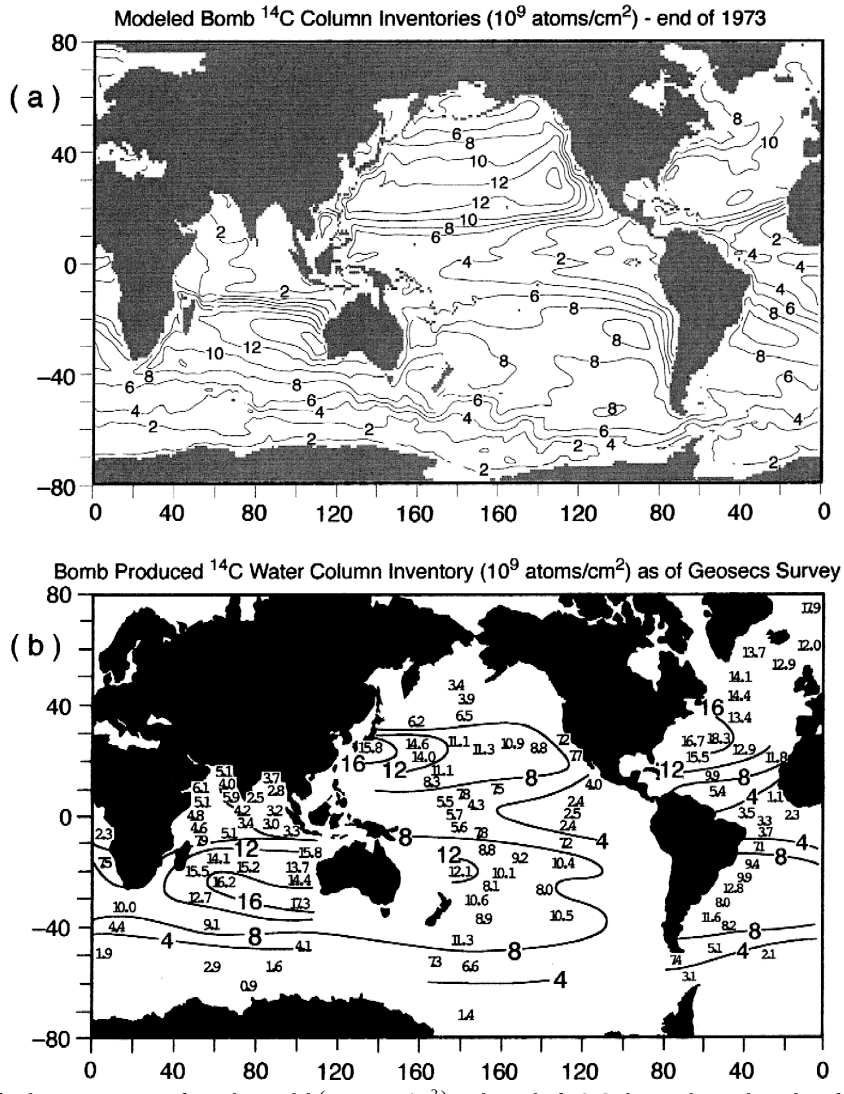

Fig. 4. A snapshot of column inventories from the model (in atoms/m^2) at the end of 1973 shown alongside a plot of inventories computed from GEOSECS data by Broecker et al. (1985). The plot of GEOSECS data is reproduced from Toggweiler et al. (1989a).

this problem, which is common to most GCMs (Toggweiler et al., 1989a; Duffy et al., 1995; Rodgers et al., 2000), to insufficient resolution; they are able to overcome it in a high (1/3°) resolution simulation of the Atlantic.

3.3. Time histories

Time histories of surface $\Delta^{14}C$ values plotted from the model (Fig. 1b) at the four different Pacific locations N, W, E and S show the characteristics of the data from the French Frigate shoals (Druffel, 1987), Nauru (Guilderson et al., 1998), Galapagos (Guilderson and Schrag, 1998), and Fiji (Toggweiler et al., 1991), respectively, shown in Fig. 1a (though site S is quite some distance from Fiji). The $\Delta^{14}C$ values in the northern subtropics peak first, followed by the southern subtropics. The tropics lag the subtropics by several years and show a progression in the timing of the peaks from west to east. The model

curves tend to rise more steeply and peak earlier and higher than the coral time series, especially in the subtropics. This seems to be a characteristic of other numerical models too. Reasons for this are discussed at the end of Section 4.3.

4. Process studies

4.1. One-dimensional processes: convection and diffusion

A simple one-dimensional model that alters the shape of an initial $\Delta^{14}C$ vertical profile over the period 1955–1995 in various ways is used to understand how convection and diffusion affect the $\Delta^{14}C$ time history. The initial profile is taken to be representative of an average prenuclear $\Delta^{14}C$ vertical distribution in the oceans. At the surface, I admit a flux of ^{14}C due to air–sea transfer computed with a constant piston velocity of 14.4 cm h^{-1} and an atmospheric $\Delta^{14}C$ value corresponding to the northern subtropics (inset, Fig. 1c). The $\Delta^{14}C$ content is mixed downward by one of two processes: (a) a constant vertical diffusivity of 10^{-5} or 10^{-4} m^2 s^{-1}, or (b) convective mixing in the top four layers (top 100 m)—a process which entails mixing the upper layer with the layer below, starting with the topmost and proceeding downward. The convective mixing is done periodically, at equally spaced time intervals. The vertical grid in this 1-D model is the same as in the MIT-GCM. It extends to 5500 m. The top four grid layers are each 25 m thick, after which the spacing increases incrementally with depth to a maximum of 500 m.

These 1-D processes affect the $\Delta^{14}C$ time histories, air–sea flux of ^{14}C, and vertical distribution of $\Delta^{14}C$ in different ways. An order of magnitude increase in diffusivity from 10^{-5} to 10^{-4} m^2 s^{-1} causes a very dramatic decrease in the surface value of $\Delta^{14}C$ (see Fig. 5a). It also results in a corresponding decrease in the vertical gradient of $\Delta^{14}C$ in the top 100 m. There is, however, no significant change in the time at which the maximum value is attained. With convective mixing (Fig. 5b) performed in the top 100 m, the maximum surface value of $\Delta^{14}C$ is lowered slightly, but more significantly, there is a systematic shift in the time at which the surface $\Delta^{14}C$ value peaks depending on whether convective mixing is performed by the model once, twice or four times each year. Table 1 summarizes the peak times of the different curves. The vertical gradient of $\Delta^{14}C$ in the upper layers is decreased as the intensity or frequency of each process is increased. One also notices that the lower layers in the model attain a maximum value later than the upper layers, and at later times in the model run, the vertical gradient in the upper four layers of the model may reverse. The exercise demonstrates that a substantial delay in peaking can indeed be caused by differences in the one-dimensional processes, and the horizontal advection of waters with a different $\Delta^{14}C$ value to a site need not be the only reason for differences in the peak times of different $\Delta^{14}C$ records.

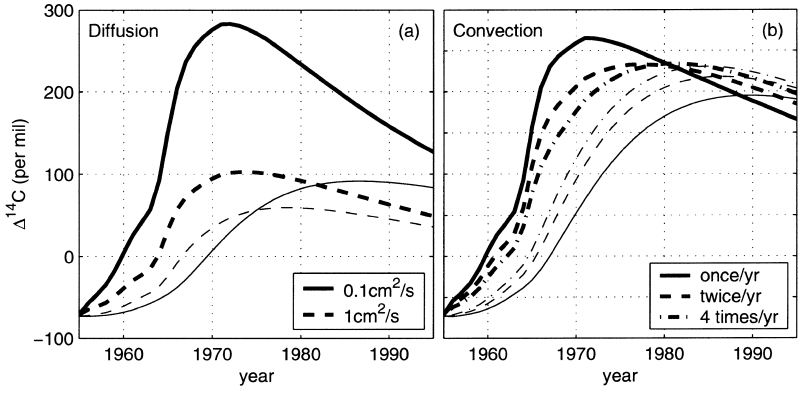

Fig. 5. The $\Delta^{14}C$ time histories in the 0–25 m top layer (thick lines) and 75–100 m 4th layer (thin lines) from the simple 1-D model (a) with different diffusivities, and (b) with convective mixing within the top 100 m.

Table 1
Maximum surface layer values of $\Delta^{14}C$, and time when the maximum rate is attained, in the simple 1-D model with diffusion and convection. Convection is restricted to the top four layers (100 m) of the water column and performed at equally-spaced intervals through the year

Process	Magnitude/ frequency	Max. $\Delta^{14}C$ value	Time of peak
Diffusion	0.1 cm^2/s	283.1	1972
Diffusion	1 cm^2/s	102.8	1974
Convective mixing	1/year	265.2	1971
Convective mixing	2/year	232.8	1977
Convective mixing	4/year	233.8	1981

We have seen that convective mixing or the deepening of the mixed layer that occurs due to local density changes and instability of the water column can have a substantial effect on the $\Delta^{14}C$ record at a site. This suggests that there is a necessity to model the mixed layer accurately in global circulation models with tracers such as radiocarbon, and accounts for the improvement in the results observed by Rodgers et al. (1997) when a variable mixed layer is used in their model. The present MIT-GCM fields used here to model $\Delta^{14}C$ were, however, generated without a mixed layer model, the depth of the mixed layer being the depth of convective mixing. Another kind of change in mixed layer depth occurs due to the change in the tilt of the thermocline as is common in the tropical Pacific ocean when the strength of the wind changes and the ocean transitions from El Niño and La Niña states. This sort of change in the mixed layer is also important to capture, and depends on an accurate representation of the dynamics, forcing and model resolution.

4.2. The role of different processes in shaping the $\Delta^{14}C$ time histories at various Pacific sites as inferred from the GCM

The rate of change of $\Delta^{14}C$ at any surface location in the model is the net sum of the change due to horizontal and vertical advection, GM mixing, vertical diffusion, convection and air–sea flux. Each process is represented by a term on the right hand side of the model Eq. (2.4), and in order to diagnose the contributions of individual process, I integrate each term in (2.4) over the period of a year at the $3 \times 3°$ square locations N, S, E and W. It should be remembered that the velocities, mixing and diffusion coefficients, convective index, and wind speeds used in the model remain the same from one year to the next. But the effective fluxes of $\Delta^{14}C$ change in time depending on its concentration and distribution.

Fig. 6a and b show the annual change in $\Delta^{14}C$ in the top 25-m surface layer boxes at locations N, S, E and W incurred due to various processes during the model run. A net positive or negative change in $\Delta^{14}C$ results in a respective rise or decline of the $\Delta^{14}C$ time history curves seen in Fig. 1b. Hence, we use this diagnostic to look for what causes the rise in the $\Delta^{14}C$ time-series curves at the tropical locations to continue longer than in the subtropics. The curves recording change in surface $\Delta^{14}C$ due to air–sea transfer are different in amplitude but similar in shape at all the locations, demonstrating that air–sea transfer cannot be the cause for the different timings of the peaks. By continuity, horizontal and vertical advection more or less compensate each other in the addition or removal of $\Delta^{14}C$ from a region (Fig. 6b), and only the imbalance between the two results in a net advective flux of $\Delta^{14}C$.

The northern and southern subtropics (Fig. 6a) show a similar distribution of $\Delta^{14}C$ gain or loss between the various processes, the north showing greater air–sea transfer and a higher intensity of all processes than the south. Convection responds quickly in removing the ^{14}C added to the surface by air–sea exchange in the subtropics, as discussed also by Sarmiento (1983) in regard to tritium. It is effective only when there is a gradient in $\Delta^{14}C$ in the near surface. The subtropics are sites of downwelling, and the downwelling constitutes a net advective flux of $\Delta^{14}C$ out of the surface layer. The vertical diffusion makes only a very small contribution in depleting the surface of $\Delta^{14}C$ when the gradients are strong.

The tropics are regions of upwelling, and the nature of the advection curves for these regions (Fig. 6b) is quite different than those of the subtropics. Initially, vertical advection depletes the surface of $\Delta^{14}C$ (the term $w\partial_z\Delta^{14}C$ is negative), but at later times, the vertical advective flux becomes positive. This indicates that while upwelling initially dilutes the surface $\Delta^{14}C$ content, at later times, the subsurface becomes enriched in $\Delta^{14}C$ relative to the surface, and the same upwelling contributes a positive $\Delta^{14}C$ flux to the surface.

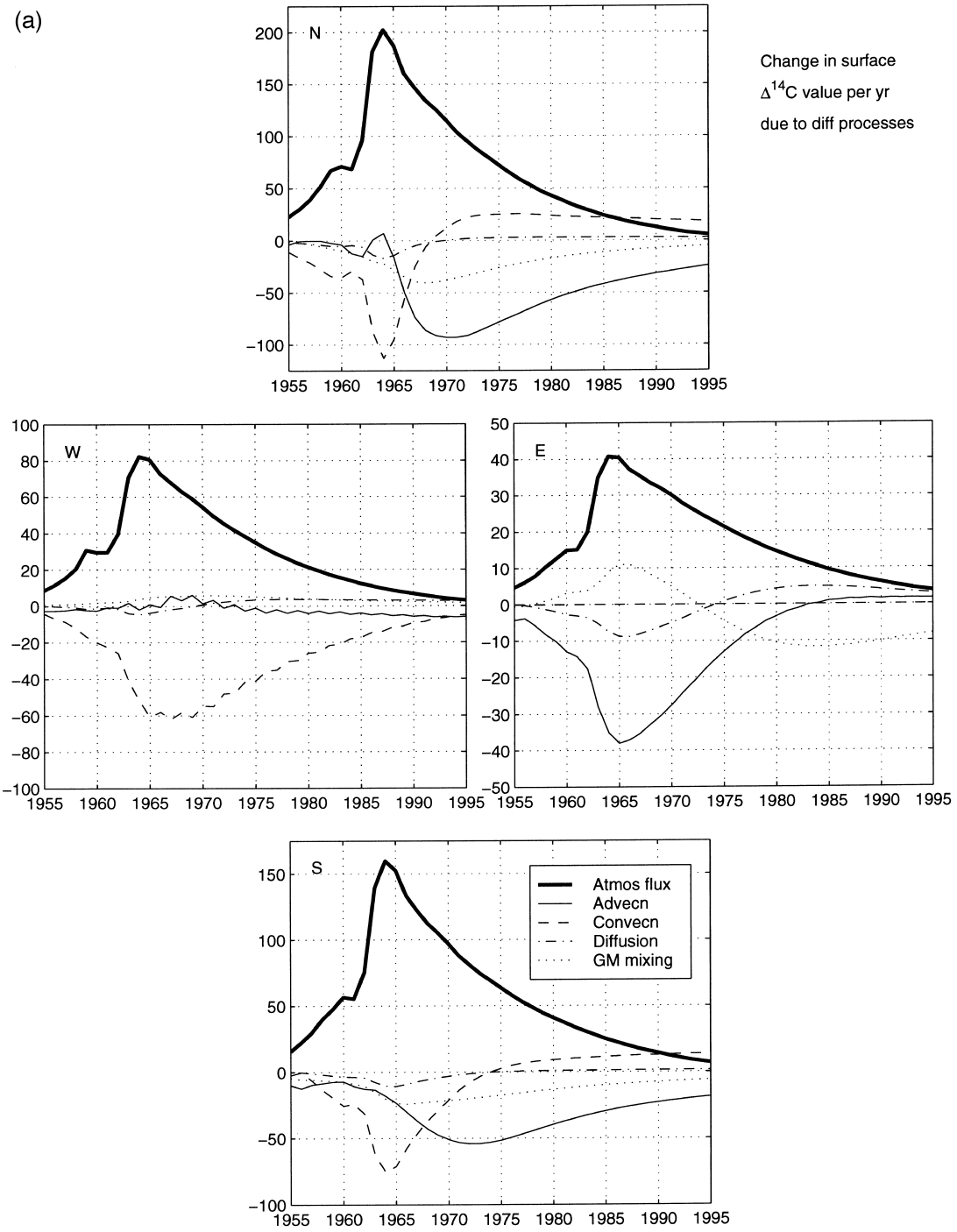

Fig. 6. (a) Annual change in surface Δ^{14}C value at the $3 \times 3°$ locations N, S, E, W marked in Fig. 1c, (a) due to various processes in the model, and (b) due to horizontal and vertical advective fluxes. The negative of the vertical advective flux is plotted to enable comparison with the horizontal flux, as only the residual of the two contributes a net advective flux. The scale on the vertical axes differs for the different locations.

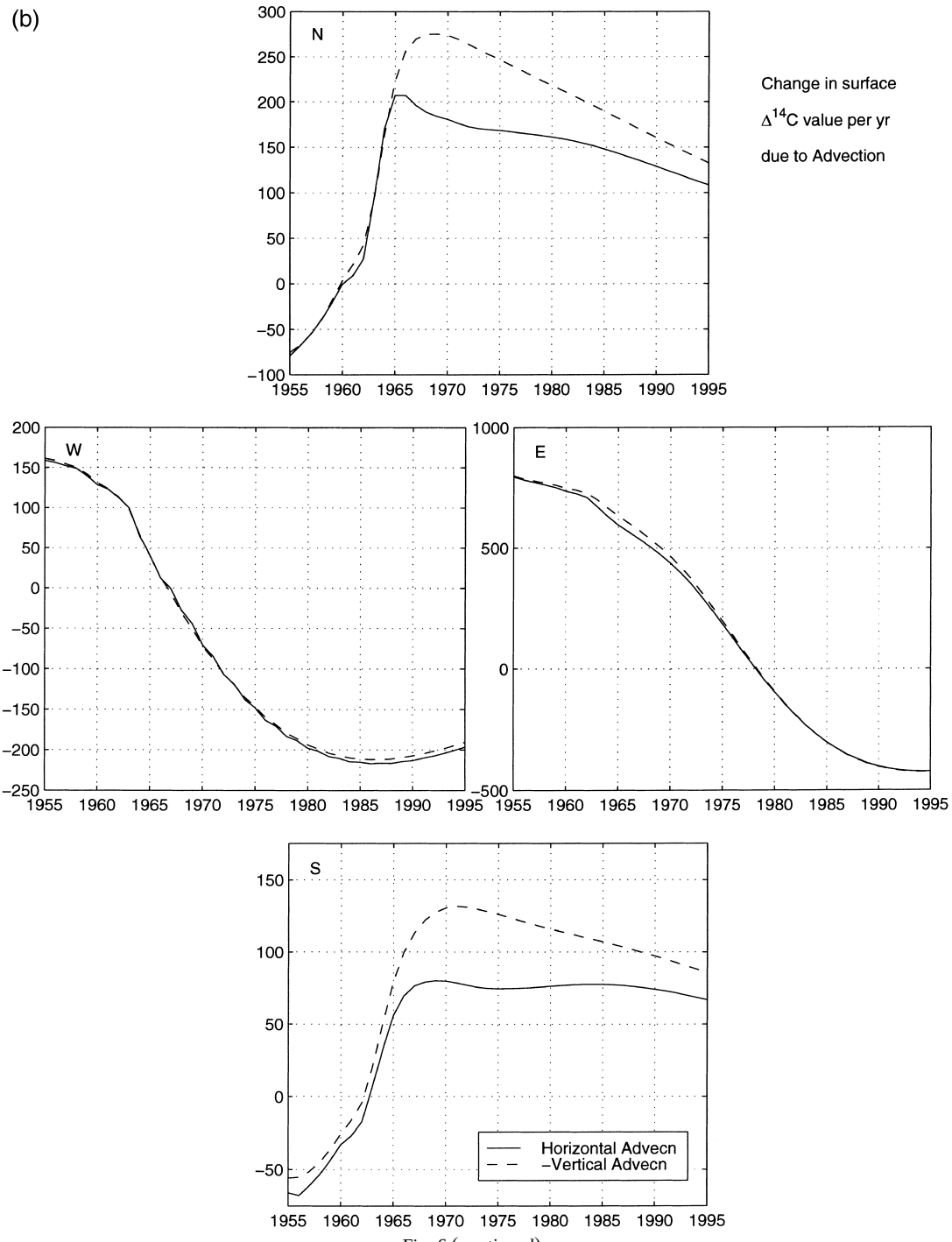

Fig. 6 (*continued*).

In the western tropics, the mixed layer is deep. In the GCM, this is represented by convective mixing between the surface and lower layers. This convection removes most of the atmospheric input of $\Delta^{14}C$

from the surface for a considerable portion of the record, and contributes to the delay in the peaking of the $\Delta^{14}C$ time history at location W (near Nauru). Diffusion has little effect.

In the eastern tropics, the mixed layer is shallow and convection has no effect at all. This is however, a region of strong upwelling, and until the beginning of the 1980s or so, the upwelling of low $\Delta^{14}C$ subsurface water dilutes the surface, resulting in a net negative advective flux of $\Delta^{14}C$ from the surface. From the 1980s onward, upwelling contributes a positive flux of $\Delta^{14}C$ to the surface as the subsurface has become enriched in $\Delta^{14}C$ relative to the surface. The vertical diffusive flux also changes from negative to positive around 1975 indicating a reversal of the $\Delta^{14}C$ gradient in the vertical.

These results suggest that in the model, the western tropical $\Delta^{14}C$ time history curves peak later than the subtropical ones, because the deep mixed layer represented by convection in the model, causes the surface input of $\Delta^{14}C$ to be distributed over a considerable depth in the western tropics. In the eastern tropics, however, convection has no effect. Thus, convection has a substantial effect in delaying the peak of surface $\Delta^{14}C$ time histories in the western tropical Pacific, it cannot explain the patterns observed in the east. In the eastern tropicical Pacific, the surface seems to get supplied with ^{14}C from the subsurface much after the peak in atmospheric influx. Since the subsurface cannot become enhanced in $\Delta^{14}C$ relative to the surface merely by a downward flux, there must clearly be a horizontal advective supply of $\Delta^{14}C$ to subsurface waters of the eastern tropics. To gain a better understanding of the lateral transport of ^{14}C, we investigate the accumulation or depletion of ^{14}C over the depth of the water column in the following section.

4.3. Inventory changes

One way of examining the contribution of horizontal advection to the $\Delta^{14}C$ value at a location is to look at the time history of the growth of the ^{14}C column inventory as compared to the addition made by the air–sea flux of ^{14}C. Using (3.7), I have computed the increment made to the column inventory each year at the locations N, S, E and W shown in Fig. 1c. Also computed is the increment to the ^{14}C inventory in the top 100 m of the water column at these locations. The inventory increment due to air–sea flux is computed from

$$\Delta I_{a-s} = F_{a-s}\Delta t \frac{\gamma_S}{1000}\Sigma C \rho N_A \Delta z \tag{4.8}$$

where ΔI_{a-s} is the increment in the column inventory at a location due to air–sea transfer (in atoms/m^2) in time interval Δt, F_{a-s} is the air–sea flux defined in (2.6), Δz is the depth over which the flux is distributed, and the other parameters are the same as in (3.7).

The time histories of yearly increments in the column inventories at locations N, S, E and W are plotted in Fig. 7. In both the northern and southern central subtropics (locations N and S), the maximum column inventory increment occurs in 1964 and is more or less coincident with the maximum in air–sea transfer. In the western tropics (location W), we observe first a maximum in total column inventory increment in 1964 that is coincident with the maximum in air–sea transfer, and then a second maximum in the total column inventory increment in 1971 that has no corresponding high in the air–sea transfer curve. The second peak that occurs in the total column inventory is not visible in the top 100-m column inventory increment curve. This indicates that a pulse of ^{14}C is added to the column inventory at a level deeper than 100 m, about 7 years after the first pulse that corresponds to the high air–sea transfer rate. Visualizing the flow field on an isopycnal surface outcropping in the subtropics shows that water from the subtropics is conveyed advectively on an isopycnal surface via the geostrophic gyre circulation and fed into the western tropical subsurface waters. Water from the subtropics is relatively rich in ^{14}C, and enriches subsurface western tropical waters as seen in Fig. 7. In the western tropics, the mixed layer is deep, and is represented in the model by the depth to which convective mixing takes place. If the ^{14}C pulse arriving from the subtropics were added within the mixed layer, it would be observable in the surface. But both the time series of surface $\Delta^{14}C$ change in Fig. 6a, and the top 100 m yearly inventory increment in Fig. 7, for site W suggest that this is not the case. The ^{14}C conveyed via the subsurface to the western tropics is fed into

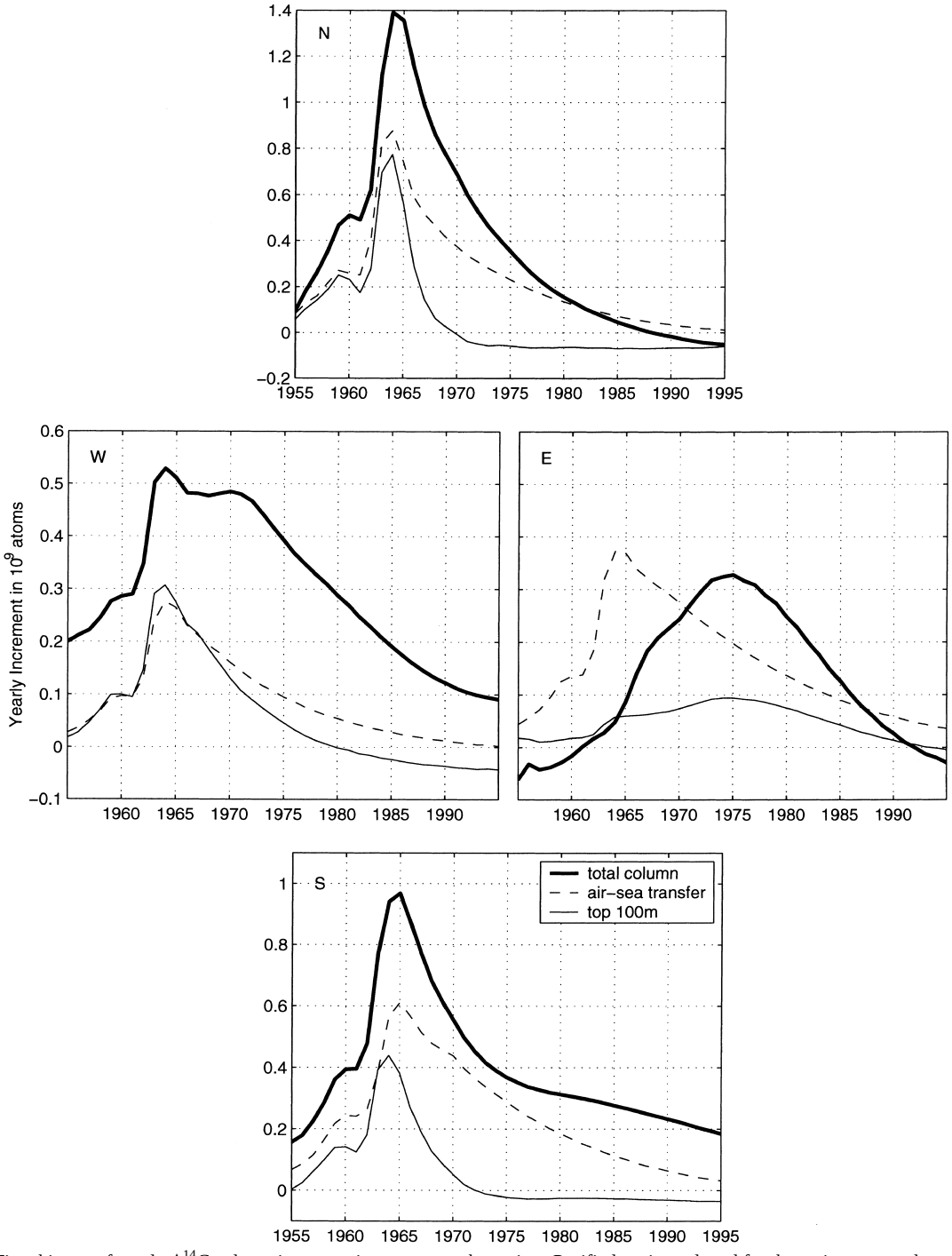

Fig. 7. Time history of yearly $\Delta^{14}C$ column inventory increments at the various Pacific locations plotted for the entire water column and for the top 100 m. Shown in dotted lines, are the time histories of the contribution to the yearly inventory increment from air–sea flux. The vertical axes have different scales at the northern, southern and equatorial sites.

the equatorial undercurrent below the mixed layer. The distance traveled by water making its way from the subtropical gyres into the western tropics is on the order of 13,000 km, and from the separation between the two peaks at location W (~8 years), one can estimate an average speed for the circulation along isopycnals to be approximately 6 cm/s.

Since the $\Delta^{14}C$ signal from the subtropics reaches the western tropics at a level deeper than the mixed layer (and deeper than 100 m), it feeds into the equatorial undercurrent that travels from west to east. In the tropics, the thermocline tilts upward from west to east on account of the easterly winds and the eastern tropics experience divergence and upwelling. At location E, the maximum increment in the ^{14}C column inventory occurs in 1975, well after the maximum in air–sea transfer. The maximum corresponds to the pulse of high ^{14}C water that originated in the subtropics, but is now conveyed via the equatorial undercurrent from the western to eastern tropics. The ^{14}C enriched undercurrent water upwells in the eastern tropics resulting in the rising trend of surface $\Delta^{14}C$ to continue long after the atmospheric peak. The lag between the second column inventory increment peak at location W and the peak at location E, is the time it takes for the $\Delta^{14}C$-rich water to be conveyed from W to E via the equatorial undercurrent. This 4-year lag in covering a distance of approximately 10,000 km indicates an approximate eastward equatorial undercurrent velocity of 8 cm/s.

The locations N, S and W show larger yearly increments in ^{14}C column inventories than the yearly ^{14}C contribution from air–sea flux. This behavior in the GCM is suspect, particularly because the subtropics (location of sites N and S) are source regions of ^{14}C where the atmospheric input ought to exceed the amount accumulated. When the yearly incremental column inventory is computed over just the top 500 m of the model and plotted along with the other curves in Fig. 7, one sees a large addition of ^{14}C to the layers between 100 and 500 m depth, coincident with the timing of the maximum atmospheric flux. This ^{14}C gain far exceeds both the annual total column inventory gain and air–sea transfer at the W, E and S sites, and is approximately equal to the total column inventory gain at site N. Moreover, it does not lag the atmospheric flux as it would if the ^{14}C were transported from another site. This behavior occurs because the model develops a spurious overshoot in the $\Delta^{14}C$ vertical profile where it abruptly changes slope (primarily between 100 and 500 m) when increased atmospheric input elevates the surface $\Delta^{14}C$ considerably relative to the subsurface. The central-difference advection scheme used in the GCM without a flux limiter, does not maintain monotonicity in the tracer when gradients become very sharp. Since this is a short-lived phenomenon coincident with the peak atmospheric flux, the model still does a good job of simulating the oceanic $\Delta^{14}C$ distribution over most of the model integration. But the increased subsurface $\Delta^{14}C$ value reduces the effectiveness of convective mixing in fluxing away surface ^{14}C exactly at the time when the surface input is large. At site N, the direction of convective flux to the surface layer gets reversed from 1968 onward, as the gradient changes sign (Fig. 6a). Thus, even though one-dimensional modeling suggests that diffusion, or a small amount of convection, is sufficient to create the observed lag between the peaks in atmospheric and sea surface time series at the subtropical locations, the sea surface $\Delta^{14}C$ time series in the GCM rise much too steeply, and peak prematurely by almost 5 years at sites N and S.

5. Conclusions

Simple one-dimensional experiments indicate that the delayed peaking of surface $\Delta^{14}C$ values at one site compared to another could occur due to greater convective mixing at that site. However, in the GCM, the short-lived elevation of $\Delta^{14}C$ in the subsurface at the time of maximal atmospheric flux due to numerical overshoot, causes a premature and heightened peak in the subtropical surface $\Delta^{14}C$ time histories. An analysis of various processes contributing to the $\Delta^{14}C$ change at different Pacific locations within the GCM framework suggests that convection, is indeed the reason for the lower and delayed peak in the $\Delta^{14}C$ time-series curve from the western tropical Pacific as compared to those from subtropical locations. In the western tropics, the mixed layer is deep, and convection distributes the ^{14}C incorporated into the surface over a substantial depth, lowering the surface $\Delta^{14}C$ and delaying the attainment of a maxi-

mum as seen in the 1-D experiments. The pattern of yearly column inventory increments from the GCM suggests that besides atmospheric influx, there is another source of ^{14}C to subsurface western tropical waters, the maximum supply occurring about 8 years after the maximum flux from the atmosphere. This pulse of ^{14}C conveyed from the subtropics is, however, infused into the western tropical waters below the mixed layer and is hardly felt at the surface. Its effect is not seen in the incremental column inventory time series computed for the top 100 m of the water column. But the ^{14}C pulse is carried eastward in the equatorial undercurrent towards Galapagos, where the thermocline surfaces and the mixed layer is practically non-existent. In the eastern tropical Pacific, upwelling of subsurface waters that are low in ^{14}C dilutes the surface during the 1950s and 1960s, thus maintaining a low $\Delta^{14}C$ value. The eastern tropics receive their largest supply of ^{14}C, both over the cumulative water column and in the upper layers, via the equatorial undercurrent approximately 13 years after they receive their maximum atmospheric flux. The late arrival and upwelling of this $\Delta^{14}C$ signal causes the surface $\Delta^{14}C$ at Galapagos to continue to rise well into the 1980s. Pictures of the flow along isopycnal surfaces that outcrop in the subtropics also suggest that subtropical surface waters rich in $\Delta^{14}C$ are subducted and carried isopycnally along pathways following the anticyclonic subtropical gyre circulation. These waters are fed into the western tropics at a few hundred meters depth, from where they are carried eastward and very gradually upward in the equatorial undercurrent to surface by upwelling in the eastern tropics. The $\Delta^{14}C$ signal can be seen to propagate from the subtropics to western tropics, and from west to east along the equator. The time lag between observed maxima in the influx to a region, enables us to compute an approximate speed of 6 cm/s for the gyre circulation and 8 cm/s for the equatorial undercurrent. The radiocarbon tracer in the GCM clearly demonstrates the subsurface pathways of transport between the subtropics, western and eastern tropics, and brings out the importance of isopycnal transport in the large-scale spreading and dissemination of tracers in the ocean. This also supports the view that the ventilation of the oceans is largely an isopycnal process.

Acknowledgements

My sincere thanks to Michael Follows, Daniel Schrag and John Marshall whose support and guidance made this work possible. I am also grateful to Alistair Adcroft and Chris Hill for their help with computing, J.R. Toggweiler and Ellen Druffel for their helpful comments and Carl Wunsch for his encouragement. I thank Charmaine King and Gordon Brown, Jr. for technical assistance.

References

Broecker, W.S., Peng, T.-H., Ostlund, H.G., Stuiver, M., 1985. The distribution of bomb radiocarbon in the ocean. J. Geophys. Res. 90, 6925–6939.

Broecker, W.S., Sutherland, S., Smethie, W., 1995. Oceanic radiocarbon: separation of the natural and bomb components. Global Biogeochem. Cycles 9 (2), 263–288.

Conkright, M.E., Levitus, S., Boyer, T.P., 1994. World Ocean Atlas 1994 Vol. 1: Nutrients, vol. 1. NOAA Atlas NESDIS 1, U.S. Department of Commerce, Washington, DC.

Deser, C., Alexander, M.A., Timlin, M.S., 1996. Upper ocean thermal variations in the North Pacific during 1970–1991. J. Clim. 9, 1840–1855.

Druffel, E.R.M., 1987. Bomb radiocarbon in the Pacific: annual and seasonal time scale variations. J. Mar. Res. 45, 667–698.

Duffy, P.B., Eliason, D.E., Bourgeois, A.J., Covey, C.C., 1995. Simulation of bomb radiocarbon in two global ocean general circulation models. J. Geophys. Res. 100 (C11), 22545–22563.

Fine, R.A., Peterson, W.H., Ostlund, H.G., 1987. The penetration of tritium into the Tropical Pacific. J. Phys. Oceanogr. 17, 553–564.

Follows, M.J., Marshall, J.C., 1996. On models of bomb $\delta^{14}C$ in the North Atlantic. J. Geophys. Res. 101 (C10), 22577–22582.

Gent, P., McWilliams, J., 1990. Isopycnal mixing in ocean circulation models. J. Phys. Oceanogr. 20, 150–155.

Griffies, S.M., 1998. The Gent–McWilliams skew-flux. J. Phys. Oceanogr. 28 (5), 831–841.

Gu, D., Philander, S.G.H., 1997. Interdecadal climate fluctuations that depend on exchanged between the tropics and extratropics. Science 275, 805–807.

Guilderson, T.P., Schrag, D.P., 1998. Abrupt shift in subsurface temperatures in the eastern tropical Pacific associated with recent changes in El Niño. Science 281, 241–243.

Guilderson, T.P., Schrag, D.P., Kashgarian, M., Southon, J., 1998. Radiocarbon variability in the Western Equatorial Pacific inferred from a high-resolution coral record from Nauru Island. J. Geophys. Res. 103, 24641–24650.

Kalnay, E., Kanamitsu, M., Kistler, R., Collins, W., Deaven, D., Gandin, L., Iredell, M., Saha, S., White, G., Woollen, J., Zhu, Y., Chelliah, M., Ebisuzaki, W., Higgins, W., Janowiak, J., Mo, K.C., Ropelewski, C., Wang, J., Leetmaa, A., Reynolds,

R., Jenne, R., Joseph, D., 1996. The NCEP/NCAR reanalysis project. Bull. Am. Meteorol. Soc. 77, 437–471.

Levitus, S., Boyer, T., 1994. World Ocean Atlas 1994 Vol. 4: Temperature, vol. 4. NOAA Atlas NESDIS 4, U.S. Department of Commerce, Washington, DC.

Marshall, J.C., Adcroft, A., Hill, C., Perelman, L., Heisey, C., 1997a. A finite-volume incompressible Navier–Stokes model for studies of the ocean on parallel computers. J. Geophys. Res. 102 (C3), 5753–5766.

Marshall, J., Hill, C., Perelman, L., Adcroft, A., 1997b. Hydrostatic, quasi-hydrostatic, and non-hydrostatic ocean modeling. J. Geophys. Res. 102 (C3), 5733–5752.

Peng, T.-H., Key, R.M., Ostlund, H.G., 1998. Temporal variations in bomb radiocarbon inventory in the Pacific Ocean. Mar. Chem. 60, 3–13.

Quay, P.D., Stuiver, M., Broecker, W.S., 1983. Upwelling rates for the equatorial Pacific ocean derived from bomb ^{14}C distribution. J. Mar. Res. 41, 769–792.

Redi, M.H., 1982. Oceanic isopycnal mixing by coordinate rotation. J. Phys. Oceanogr. 12, 1154–1158.

Rodgers, K.B., Cane, M.A., Schrag, D.P., 1997. Seasonal variability of sea surface $\delta^{14}C$ in the equatorial Pacific in an ocean circulation model. J. Geophys. Res. 102 (C8), 18627–18639.

Rodgers, K.B., Schrag, D.P., Cane, M.A., Naik, N.H., 2000. The bomb ^{14}C transient in the Pacific Ocean. J. Geophys. Res. 105 (C4), 8489–8512.

Sarmiento, J.L., 1983. A simulation of bomb tritium entry into the Atlantic Ocean. J. Phys. Oceanogr. 13, 1924–1939.

Stuiver, M., Polach, H.A., 1977. Discussion: reporting of ^{14}C data. Radiocarbon 19 (3), 355–363.

Stuiver, M., Ostlund, H.G., McConnaughey, T.A., 1981. GEOSECS Atlantic and Pacific ^{14}C distribution. In: Bolin, B. (Ed.), Scope 16. Carbon Cycle Modeling. Wiley, New York, pp. 131–157.

Toggweiler, J.R., Carson, S., 1995. What are upwelling systems contributing to the ocean's carbon and nutrient budgets? In: Summerhayes, C.P., Emeis, K.C., Angel, M.V., Smith, R.L., Zeitzschel, B. (Eds.), Upwelling in the Ocean: Modern Processes and Ancient Records. John Wiley and Sons, Ltd., pp. 337–360.

Toggweiler, J.R., Dixon, K., Bryan, K., 1989a. Simulations of radiocarbon in a coarse-resolution world ocean model: 2. Distributions of bomb-produced carbon 14. J. Geophys. Res. 94 (C6), 8243–8264.

Toggweiler, J.R., Dixon, K., Bryan, K., 1989b. Simulations of radiocarbon in a coarse-resolution world ocean model: 1. Steady state prebomb distributions. J. Geophys. Res. 94 (C6), 8217–8242.

Toggweiler, J.R., Dixon, K., Broecker, W.S., 1991. The Peru upwelling and the ventilation of the South Pacific thermocline. J. Geophys. Res. 96 (C11), 20467–20497.

Veronis, G., 1975. The role of models in tracer studies. Numerical Models of the Ocean Circulation. National Academy of Sciences, Washington, DC, pp. 133–146.

Wanninkhof, R., 1992. Relationship between wind speed and gas exchange over the ocean. J. Geophys. Res. 97 (C5), 7373–7382.

Wunsch, C., 1984. An estimate of the upwelling rate in the equatorial Atlantic based on the distribution of bomb radiocarbon and quasi-geostrophic dynamics. J. Geophys. Res. 89 (C5), 7971–7978.

Zhang, R.-H., Rothstein, L.M., Busalacchi, A.J., 1998. Origin of upper-ocean warming and El Niño changes in the tropical Pacific Ocean. Nature 391, 879–883.